Wavelets in High-Capacity DWDM Systems and Modal-Division Multiplexed Transmissions

Andrés Macho, *Student Member, IEEE*

Abstract— Optical communications receivers using wavelet signals processing is proposed in this paper for dense wavelength-division multiplexed (DWDM) systems and modal-division multiplexed (MDM) transmissions. The optical signal-to-noise ratio (OSNR) required to demodulate polarization-division multiplexed quadrature phase shift keying (PDM-QPSK) modulation format is alleviated with the wavelet denoising process. This procedure improves the bit error rate (BER) performance and increasing the transmission distance in DWDM systems. Additionally, the wavelet-based design relies on signal decomposition using time-limited basis functions allowing to reduce the computational cost in Digital-Signal-Processing (DSP) module. Attending to MDM systems, a new scheme of encoding data bits based on wavelets is presented to minimize the mode coupling in few-mode (FWF) and multimode fibers (MMF). The Shifted Prolate Wave Spheroidal (SPWS) functions are proposed to reduce the modal interference.

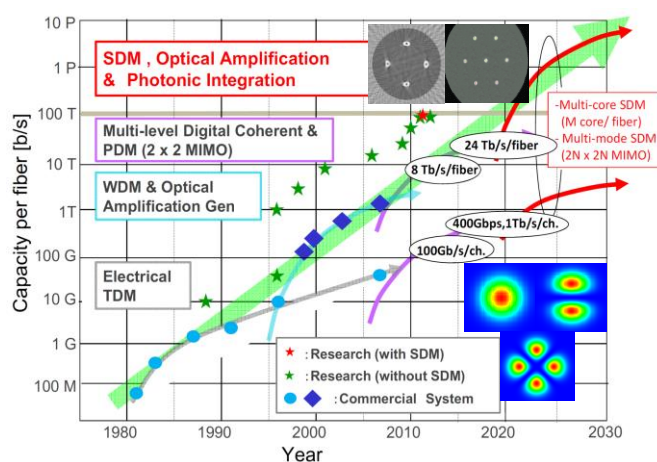*Index Terms*— Digital communications, digital signal processing (DSP), DWDM, MDM, wavelet transform.

Fig. 1. Evolution of single-channel capacity during the last two decades and aggregate capacities. This figure has been modified for this work from reference [60].

I. INTRODUCTION

WITH the vast growth of network traffic over the past two decades it has become increasingly important to realize an ultrahigh-speed backbone network. The amount of traffic carried on backbone networks has been growing exponentially at about 30 to 60% per year, and now the increasing number of applications relying on machine-to-machine traffic and cloud services is accelerating the growth of bandwidth requirements near to 90% per year [7], [37], [62].

Over the past twenty years, the demand for communication bandwidth has been economically met by wavelength-division multiplexed (WDM) optical transmission systems. A series of technological breakthroughs have allowed the capacity-per-fiber to increase around 10x every four years, as illustrated in Figure 1. Transmission technology has therefore thus far been able to keep up with the relentless, exponential growth of capacity demand. The cost of transmitting exponentially more data was also manageable, in large part because more data was transmitted over the same fiber by upgrading equipment at the fiber ends. Fig. 1 illustrates the evolution of single-channel bit rates (single-carrier, single-polarization, electronically multiplexed; circles), as well as of aggregate per-fiber capacities using wavelength-, polarization-, and most recently space-division multiplexing (SDM) [57].

As can be seen from Fig. 1, WDM was able to boost the relatively slow progress in single-channel bit rates [62]. The

figure indicates that, in spite of relatively slow progress on the single-channel bit rate, a larger WDM capacity, supported by the increase in spectral efficiency, had been achieved by around 2002. This was, basically, made possible by employing a closer channel spacing. Consequently, by 2002 high-speed fiber-optic systems research had started to investigate new modulation formats using direct detection and Fourier approach based in harmonic functions decomposition [56].

However, with the view focused in 100-Gb/s transmissions and beyond [63], it became clear that additional techniques were needed to use 100-Gb/s channels in the widely established 50-GHz WDM infrastructure [57]. In this context, polarization-division multiplexed (PDM) allowed for a reduction of symbol rates, which brought 40 and 100-Gb/s optical signals. At this point coherent optical receivers emerged as the main area of interest in broadband optical communications due to the high receiver sensitivities which they can achieve. They have since been combined with digital post-processing to perform all-electronic CD and PMD compensation, frequency- and phase locking, and polarization demultiplexing [43]. The use of coherent optical receivers with the combination of advanced modulation formats has led to increase the long transmission distances and high spectral efficiencies required for the current commercial core DWDM networks.

But in the coming decade, as optical transmission systems operating over single strands of legacy single-mode fiber

(SMF) are reaching their fundamental capacity limits [17], SDM based in modal-division multiplexing (MDM) and multicore fibers (MCF) is likely to become a critical technology to meet future traffic demands. However, attending exclusively to MDM systems, the inability to individually excite and detect each propagation mode lets modal dispersion within each mode group still limit the bandwidth-distance product of such systems, which makes them unattractive for long-haul transmission [35, Ch. 10].

As we have mentioned above, DWDM and SDM systems are based in Fourier signal processing, which decomposes signals in harmonic functions. In this paper, we propose the wavelet approach based in time-limited basis functions for DWDM and MDM systems. In the former, the use of wavelets let us to reduce the DSP complexity and increase the sensitivity of the coherent receiver. In the latter, the wavelet approach is an opportunity to increase the bandwidth-distance factor due to the reduction of the mode coupling and the OSNR required for QPSK modulation format limited by ASE noise [24].

The paper is organized as follows. Section II reviews the mathematic fundamentals of the wavelet transform, Section III focuses in wavelet applications for DWDM and MDM systems, Section IV describes a wavelet-based FIR filter design used for backward-propagation to nonlinear compensation in the DSP of the coherent receivers and Section V presents the future perspectives, the open issues and it contains an implementation of the continuous wavelet transform in the optical domain. Finally, in Section VI the paper concludes with a discussion of the main results obtained in this work.

II. WAVELET PACKET TRANSFORM FUNDAMENTALS

It is instructive to start our discussion with the Fourier transform that is more well-known in optical communications than the wavelet transform. The Fourier transform is an operation that transforms one complex-valued function into another. Since the original function is typically of time-domain and the new function is of frequency-domain, the Fourier transform is often called the frequency-domain representation of the original function. Discrete Fourier transform (DFT) is a specific kind of Fourier transform that requires the input function be discrete, which means its non-zero values have a finite duration. Mathematically, forward and inverse DFTs are defined as (N-order):

$$X(k) = DFT^N\{x[n]\} = \sum_{n=0}^{N-1} x[n]e^{-j2\pi nk/N} \quad (1)$$

$$x[n] = IDFT^N\{X(k)\} = \frac{1}{N}\sum_{k=0}^{N-1} X(k)e^{+j2\pi nk/N} \quad (2)$$

It is known that DFT only has frequency localization, and its basis functions, the sinusoids are infinitely long in time domain. In comparison, the wavelet transform is the representation of a function by an orthogonal set called "*wavelets*". It is another form of time-frequency representation

for the original function. The more important differences between the wavelet transform and the Fourier transform are two:

- Wavelet transform is based in non-harmonic functions. In this case, the basic functions of the vector space $\mathcal{F}(\mathbb{R}, \mathbb{C})$ are localized in both time and frequency, in contrast with harmonic functions of Fourier transform, which are completely delocalized in time.

- To describe finer details in time, wavelet expansion uses scaled basis functions, contrary to Fourier analysis, which uses higher frequencies. This is the key to reduce in Section IV the DSP complexity to compensate the signal degradation due to fiber Kerr nonlinearities. Therefore, we could decompose a temporal event that occurs briefly only once using only a few wavelet basis functions rather than hundreds of Fourier components.

Any square integrable function $\psi(t)$ (that is, *finite energy*) can be a wavelet if it satisfies (in addition to a few other conditions) the admissibility condition:

$$C_\psi = \int_0^{+\infty} \frac{|\widehat{\Psi}(\omega)|^2}{\omega} d\omega < \infty \quad (3)$$

where $\widehat{\Psi}(\omega)$ is the Fourier transform of $\psi(t)$. If the function ψ satisfies (3) we say that $\psi \in L^2(\mathbb{R}, \mathbb{C})$, which is the vector space of square integrable functions. A (much) less mathematically stringent way of saying the same thing is to describe a wavelet as a few oscillations on a finite interval. If $\psi(t)$ is the mother wavelet, we can create a whole family of wavelets by scaling and shifting the original mother wavelet:

$$\psi_{ab}(t) \stackrel{\text{def}}{=} \frac{1}{\sqrt{2}}\psi\left(\frac{t-b}{a}\right) \quad (4)$$

where a is the scaling parameter and b is the shift parameter, both real parameters varying continuously from $-\infty$ to $+\infty$. The family $\psi_{ab}(t)$ can generate the whole vector space $L^2(\mathbb{R}, \mathbb{C})$, so an arbitrary signal $f(t) \in L^2(\mathbb{R}, \mathbb{C})$ can be written as a function of the basic functions as follow [11], [31]:

$$f(t) = \frac{1}{C_\psi} \iint_{-\infty}^{+\infty} CWT_f(a,b)\psi\left(\frac{t-b}{a}\right)\frac{1}{a^2} da db \quad (5)$$

where the scalar numbers of this linear combination $CWT_f(a,b)$ are known as the continuous wavelet transformation (CWT), corresponding to the module of the projection of $f(t)$ over the vector sub-space generated by the axis $\psi_{ab}(t)$:

$$CWT_f(a,b) = \left\|\overrightarrow{proy\left(\overrightarrow{f(t)}\right)}_{L\left(\{\overrightarrow{\psi_{ab}(t)}\}\right)}\right\|_2 =$$

$$= \frac{\left\langle \overrightarrow{f(t)}, \overrightarrow{\psi_{ab}(t)} \right\rangle}{\left\langle \overrightarrow{\psi_{ab}(t)}, \overrightarrow{\psi_{ab}(t)} \right\rangle} = \frac{1}{\sqrt{|a|}} \int_{-\infty}^{+\infty} f(t)\psi_{ab}^*(t)dt \quad (6)$$

To perform the WT in a DSP we need to work with digital sequences $f[n]$, so it is necessary to create the discrete version of the CWT: the discrete wavelet transformation (DWT) [1]. In order to explain this mathematical tool, we first explain an approximation of the expressions of DWT, and later we write the exactly expressions with the Haar mother wavelet function.

In the CWT, a and b can vary continuously, but the resulting family of wavelets will not all be orthogonal to each other. To work with digital sequences (and similar to DFT) it is necessary to obtain a set of basic functions. To create a whole family of orthogonal wavelets, a proposal is to vary a and b parameters discreetly according to the dyadic scale:

$$a = 2^k; b = m2^k \quad (7)$$

using a fixed time-sampling interval of 1 and a constant ratio between two consecutively scaled wavelets of 2. The time-sampling rate thus automatically adjusts to the scale. With this operation we obtain the basic function $\psi_{km}[n]$ given by:

$$\psi_{km}[n] = \psi\left(\frac{n}{2^k} - m\right) \quad (8)$$

and we can now use these discretely scaled and shifted wavelets as a complete orthonormal set of basic functions to describe an arbitrary digital signal $f[n]$ with:

$$f[n] = \frac{1}{C_\psi} \sum_k \sum_m DWT_f(k,m) \cdot \frac{1}{2^{2k}} \cdot \psi_{km}[n] \quad (8)$$

Similar to (6) the scalar numbers of this linear combination are given by the DWT of $f[n]$. DWT can be viewed as the module of the projection of $f[n]$ over the vector sub-space generated by the axis $\psi_{km}[n]$:

$$DWT_f(k,m) = \left\| \overrightarrow{proy\left(\overrightarrow{f[n]}\right)}_{L\left(\left\{\overrightarrow{\psi_{km}[n]}\right\}\right)} \right\|_2 =$$

$$= \frac{\left\langle \overrightarrow{f[n]}, \overrightarrow{\psi_{km}[n]} \right\rangle}{\left\langle \overrightarrow{\psi_{km}[n]}, \overrightarrow{\psi_{km}[n]} \right\rangle} = \frac{1}{\sqrt{2^k}} \sum_{n=-\infty}^{+\infty} f[n] \cdot \psi_{km}^*[n] \quad (9)$$

If this were traditional Fourier analysis, $DWT_f(k,m)$ would correspond to the Fourier coefficients and $\psi_{km}[n]$ would correspond to the harmonic function $e^{+jk\omega n}$ of eq. (2). The DWT of a signal can be efficiently computed using discrete-time filter banks that are either infinite-time response (IIR) or finite time response (FIR) filters. It can be implemented through the methodology known as Multiresolution Analysis (MRA) [41].

In the next lines we will explain the exactly expressions of the DWT and the discrete wavelet decomposition with a

practical example: the Haar wavelet [41]. Haar wavelet function $\psi(t)$ is:

$$\psi(t) = \begin{cases} 1 & 0 \leq t < 1/2 \\ -1 & 1/2 \leq t < 1 \\ 0 & otherwise \end{cases} \quad (10)$$

an its scaling function is:

$$\varphi(t) = \begin{cases} 1 & 0 \leq t < 1 \\ 0 & otherwise \end{cases} \quad (11)$$

The filter coefficients of Haar wavelet can be obtained knowing the relations (12) and (13):

$$\varphi(t) = \sum_{n=-\infty}^{+\infty} \sqrt{2} \cdot h[n]\varphi(2t - n) \quad (12)$$

$$\psi(t) = \sum_{n=-\infty}^{+\infty} \sqrt{2} \cdot g[n]\varphi(2t - n) \quad (13)$$

and consequently:

$$h[n] = \frac{1}{\sqrt{2}}(-1,1); \quad g[n] = \frac{1}{\sqrt{2}}(1,1) \quad (14)$$

Now we have defined scaling and wavelet function as well as scaling and wavelet coefficients. From the wavelet theory we know that for any arbitrary signal we can expand it into a sum of scaling and wavelet functions, and this process is called discrete wavelet decomposition. The discrete wavelet expansion of any signal $f \in L^2(\mathbb{R}, \mathbb{C})$ is given by [41]:

$$f[n] = \sum_{m=-\infty}^{+\infty} c_{k_0}(m) \cdot \varphi_{k_0,m}[n] + \sum_{m=-\infty}^{+\infty} \sum_{k=k_0}^{+\infty} d_k(m) \cdot \psi_{km}[n]$$

$$(15)$$

for $k, m \in \mathbb{Z}$ and k_0 is an arbitrary integer. It can be seen that k and m provide the frequency (or scale) and time localization, respectively. The coefficients $c_{k_0}(m)$, known as detail coefficient; and $d_k(m)$, known as approximation coefficient, can be obtained with the same criteria as (6) and (9):

$$c_{k_0}(m) = \left\| \overrightarrow{proy\left(\overrightarrow{f[n]}\right)}_{L\left(\overrightarrow{\varphi_{k_0,m}}\right)} \right\|_2 =$$

$$= \frac{\left\langle \overrightarrow{f[n]}, \overrightarrow{\varphi_{k_0,m}[n]} \right\rangle}{\left\langle \overrightarrow{\varphi_{k_0,m}[n]}, \overrightarrow{\varphi_{k_0,m}[n]} \right\rangle} = \sum_{n=-\infty}^{+\infty} f[n] \cdot \varphi_{k_0,m}^*[n] \quad (16)$$

$$d_k(m) = \left\| \overrightarrow{proy\left(\overrightarrow{f[n]}\right)}_{L\left(\overrightarrow{\psi_{km}}\right)} \right\|_2 =$$

$$= \frac{\left\langle \overrightarrow{f[n]}, \overrightarrow{\psi_{km}[n]} \right\rangle}{\left\langle \overrightarrow{\psi_{km}[n]}, \overrightarrow{\psi_{km}[n]} \right\rangle} = \sum_{n=-\infty}^{+\infty} f[n] \cdot \psi_{k,m}^*[n] \quad (17)$$

where the scaling functions $\varphi_{k_0,m}$ and the wavelets functions $\psi_{k,m}$ are given by the follow expressions:

$$\varphi_{k_0,m}[n] = \sqrt{2^{k_0}} \cdot \varphi[2^{k_0}n - m] \qquad (18)$$

$$\psi_{k,m}[n] = \sqrt{2^k} \cdot \psi[2^k n - m] \qquad (19)$$

Combing (12) with (16) and (13) with (17), following relationship can be deduced [11]:

$$c_k(m) = \sum_{n=-\infty}^{+\infty} h[n - 2m]c_{k+1}(n) \qquad (20)$$

$$d_k(m) = \sum_{n=-\infty}^{+\infty} g[n - 2m]c_{k+1}(n) \qquad (21)$$

In practical applications and for computational efficiency, one prefers a wavelet with compact support where the scaling function $\varphi(t)$ and wavelet mother function $\psi(t)$ can be considered finite in length. Detailed filter bank implementation of the DWT algorithm is as follows: To start the DWT, one needs to get the detail coefficients $c_k(m)$ at high resolution and for high enough scale the scaling function, $\varphi_k[n]$ acts as delta function with the inner product as a sampling of $f[n]$ according to (16). Therefore, the samples of $f[n]$ are passed through a low-pass filter (scaling filter) g and high-pass filter (wavelet filter) h simultaneously, resulting in a convolution of the two. The two filters are related to each other and they are known as a quadrature mirror filter (QMF); the filter outputs are then down-sampled by 2 since half the frequencies of the signal have been removed, half of the samples can be discarded according to Nyquist's theory; the outputs will give the detail coefficients $c_k(m)$ (from the high-pass filter h) and the approximation coefficients $d_k(m)$ (from the low-pass filter g) as we show from (20) and (21); this decomposition process can be repeated to further increase the frequency resolution, but only the approximation coefficients are decomposed. The above implementation of algorithm can be represented as a lower-half binary tree structure as shown in Fig. 2. It is important to notice that for a 2^N-point DFT, the bandwidth is uniformly divided. However for an n-level DWT, the bandwidth is logarithmically divided since only half of the spectrum—the lowpass filter outputs are decomposed at each level. An explicit comparison of the bandwidth division feature between DFT and DWT is shown in Fig. 3.

III. BER IMPROVEMENT IN DWDM AND MDM SYSTEMS

Wavelet signal processing for DWDM and MDM systems are proposed with two different points of view in this paper. In this section we analyze the first approach, meanwhile the second proposal is taken into account in the next section:

1) ASE noise filtering at the receiver improving the SNR when PDM-QPSK modulation format is used [24], [36].
2) Reduction of the number of operations required for digital backward-propagation used for nonlinear impairments compensation [20]-[22].

According to Ge's studies, a significant BER performance improvement can be obtained if the matched filter of the
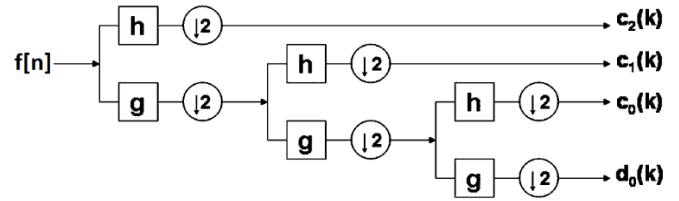

Fig. 2. Block diagram of a discrete wavelet transform (DWT) with 3-level filter banks. ↓ 2 stands for two times downsampling. $f(t_i)$ at the input is the sampled input signal $f(t)$. This figure is inserted from reference [41].
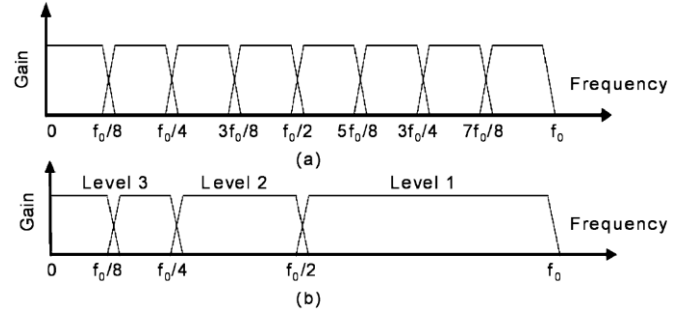

Fig. 3. Evolution of single- (a) Fourier transforms with uniform division of bandwidth. (b)Wavelet transforms with logarithmic division of bandwidth. This figure is inserted from reference [41].

receiver is preceded by a wavelet denoising operation (Fig. 4) [24]. In that work QPSK signal is transmitted in the presence of Additive White Gaussian Noise (AWGN). Wavelet-domain decomposition of the received signals is carried out via the DWT and (MRA) [41]. The Haar, Daubechies5, Coiflet5 and Symmlet4 wavelets were used, along with a soft-thresholding technique.

The improvements realized by matched filter-based demodulation in conjunction with the use of wavelet thresholding techniques are shown in Fig. 5. It shows the BER performance as a function of the SNR per bit (E_b/N_0). The BER improvement has been found in [36] and verified in [24]. Using the Daubechies5 and Haar wavelets and wavelet thresholding methods improvements in BER of over three orders of magnitude are achievable within the range of E_b/N_0 from -5 dB to 8 dB as demonstrated in Fig. 5.

The experimental evidence obtained via simulation clearly indicates that the additive noise process affecting the signal after matched filtering is shown to have a Gaussian distribution that possesses much smaller variance. Hence, the pre-detection SNR is effectively increased by action of the wavelet-domain de-noising operation. The simulation evaluation in [24] of the overall system BER accurately predicts the improved performance of the matched filter detector when used in conjunction with wavelet-domain denoising.

A. Wavelets in DWDM Systems

Attending to its application in PDM-QPSK DWDM systems, we propose to improve the performance obtained in our works [44], [52], [53] and [43]. Before that, however, it is necessary to describe the modified coherent optical receiver with wavelet processing employed in our simulations. In coherent optical communication, information is encoded onto the electrical field of the lightwave; decoding entails direct
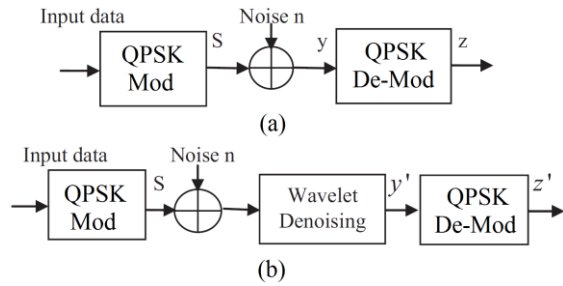
Fig. 4. (a) Structure of a matched filter-based typical QPSK communications system. (b) Structure of the QPSK system employing wavelet-based de-noising. This figure is inserted from reference [24].
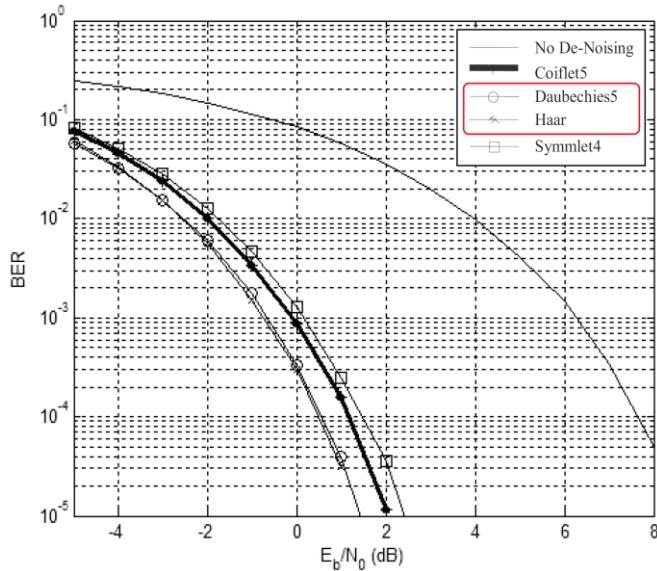

Fig. 5. BER curves for QPSK signals using different wavelets in the de-noising operation. This figure is inserted from reference [24].

measurement of the complex electric field. To measure the complex electric field of the lightwave, the incoming data signal (after fiber transmission) interferes with a local oscillator (LO) in an optical 90° hybrid [35]. If the balanced detectors in the upper branches measure the real part of the input data signal, the lower branches, with the LO phase delayed by 90°, will measure the imaginary part of the input data signal. For reliable measurement of the complex field of the data signal, the LO must be locked in both phase and polarization with the incoming data. Both phase and polarization management can be realized in the electrical domain by using DSP. In a digital coherent receiver, there are four key subsystems:

1) Optical front-end, which linearly maps the optical field into a set of electrical signals.
2) ADC, which converts from the electrical signals into a set of discrete-time-quantized signals at the sampling rate.
3) The DSP, which process the digital samples into a set of signals at the symbol rate.
4) Outer receiver, which includes error correction and whose functionality is to optimally decode the demodulated signals in order to produce the best estimate of the sequence of bits, which were encoded by the transmitter.

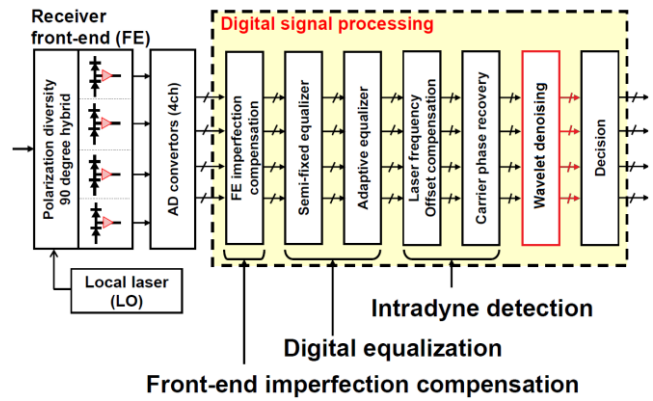The main modification is performed inside the DSP, which

Fig. 6. Different subsystems of a digital coherent optical receiver.

Modulation Format Coherent Detection	OSNR$_{req}$ (BER$_{ref}$=10^{-12} FEC=0%) 100 Gb/s	OSNR$_{req}$ (BER$_{ref}$=10^{-12} FEC=0%) 200 Gb/s
PDM-NRZ-(D)QPSK	21,0 dB	24,9 dB
PDM-67%RZ-(D)QPSK	20,3 dB	24,2 dB
PDM-50%RZ-(D)QPSK	20,2 dB	24,1 dB
PDM-33%RZ-(D)QPSK	19,8 dB	23,7 dB
PDM-CSRZ-(D)QPSK	20,2 dB	24,1 dB

Table I. Sensitivity of PDM-(D)QPSK signals (0.1-nm resolution bandwidth) without wavelet denoising [44].

Modulation Format Coherent Detection	OSNR$_{req}$ (BER$_{ref}$=10^{-12} FEC=0%) 100 Gb/s	OSNR$_{req}$ (BER$_{ref}$=10^{-12} FEC=0%) 200 Gb/s
PDM-NRZ-(D)QPSK	9,7 dB	13,6 dB
PDM-67%RZ-(D)QPSK	9,1 dB	13,0 dB
PDM-50%RZ-(D)QPSK	8,9 dB	12,8 dB
PDM-33%RZ-(D)QPSK	8,5 dB	12,4 dB
PDM-CSRZ-(D)QPSK	8,9 dB	12,9 dB

Table II. Sensitivity of PDM-(D)QPSK signals (0.1-nm resolution bandwidth) with wavelet denoising preceding the matched filter of the receiver [44].

is showed in Fig. 6. The wavelet denoising subsystem is included between the carrier phase estimator and the matched filter of the symbol decisor (symbol-by-symbol detection has been supposed) according to [24]. It is also interesting to note that the DSP implements the automated learning concept [35], [43], [59] to compensate the crosstalk between the two received polarizations (PMD compensation and polarization demultiplexing) following the variations in the state-of-polarization of the optical fiber. A full description of the main subsystems in an optical coherent receiver can be found in [16], [43] and [47].

As we have mentioned above, our proposal is to use this optical receiver with wavelet processing to improve the results obtained in [44], [52], [53] and [43]. In the first reference, we studied the sensitivity variation of PDM-QPSK format with the pulse shaping. Table I summarizes the results measured in
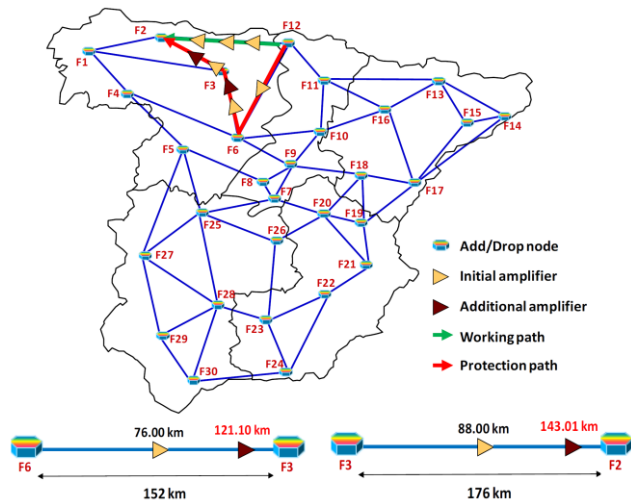
Fig. 7. Telefónica I+D's Spanish network model showing a traffic demand between nodes F12 and F2 for working and protection paths. Two additional amplifiers are deployed on two links (F6-F3 and F3-F2) [52].

100 and 200-Gb/s transmissions with coherent detection. In Table II we have recalculated the above results including the wavelet denoising operation preceding to the matched filter of the coherent receiver. We can see that for a BER reference (BER$_{ref}$) of 10^{-12} the required OSNR (OSNR$_{req}$) is relaxed around ~11.3 dB.

In [52] and [53] we aimed at evaluating the possible energy and spectral benefits that could be achieved by the deployment of additional optical amplifiers in the Spain national optical network (the simulation scenario is shown in Fig. 7). The envisioned traffic growth is forcing operators to find new approaches to achieve a better utilization of the scarce spectrum and energy resources. In these papers we proposed to add new amplifiers in some ligthpaths to improve the received OSNR allowing the migration from 4C-100G-PDM-QPSK transponders to 2C-200G-PDM-16QAM transponders. We simulated this migration in a working path (F12-F2 nodes) and in its correspondent protection path (F12-F6-F3-F2). The results concluded that our approach can enhance the energy efficiency per GHz of the network up to 74%.

Now, we propose to recalculate the above simulations using the wavelet approach with the 4C-100G-PDM-QPSK transponders. The objective is to analyze which strategy provides more energy efficiency: 4C-100G-PDM-QPSK with wavelet denoising or 2C-200G-PDM-16QAM with additional optical amplifiers in the ligthpaths. Simulating the protection path (as depicted in Fig. 7) adding two new erbium doped fiber amplifiers (EDFA) according to [52], it is possible to improve the received OSNR level from 22.96 dB to 26.73 dB, making possible the utilization of 400 Gbps transmission (26.73 dB > 23.5+3 dB), with a received power of -7 dBm, well above the receiver sensitivity. Therefore, the power consumption can be reduced by using 2x200 Gbps lightpaths instead of 4x100Gbps, as follows:

- Power consumption without additional amplifiers:
  4x243.4 W=973.6W

- Power consumption with two additional amplifiers:
  2x240.95 W+2x170W=821.9 W

- Total power reduction:
  10log(973.6W/821.9 W)=0.74 dB

However, maintaining the transponder technology 4C-100G-PDM-QPSK and employing wavelet denoising (Haar and Daubechies5), the OSNR$_{req}$ for a BER$_{ref}$ =10^{-3} (FEC limit) is reduced in ~7 dB (Fig. 5, $\Delta OSNR = \Delta SNR_{bit}$). Consequently, the four carriers PDM-QPSK can be launched to the fiber with 1dBm-7dB = -6dBm per carrier. The power consumption is reduced in 7 dB+10log(4) = 13.02 dB without additional amplifiers, in contrast with the 0.74 dB obtained in [52] and [53]. The main disadvantage is an increment in the receiver complexity.

In [43] we presented two high-spectral-efficiency and high-speed DWDM transmission simulations using PDM-QPSK modulation format. In this paper the goal is to insert the wavelet denoising processing in these simulations to compare the results obtained in both works.

➤ *2.24 Bit/s/Hz, 1500 km, 40 x 112-Gb/s PDM-NRZ-QPSK*

Figure 8 shows the simulation scenario. At the transmitter, 40 wavelengths (1550–1565.64 nm [29]) are modulated by two 112-Gb/s PDM-NRZ-QPSK modulators (for odd and even channels), each modulating twenty 100 GHz spaced wavelengths. The odd and the even channels are combined by using an optical adder (ideal multiplexer). The 40 channels originate from an external cavity laser (ECL) array, with a linewidth of 50 kHz to reduce the laser phase noise at the receiver. Even and odd channels are individually modulated using a conventional quadrature modulator for each polarization [36] and polarization-division multiplexed by a polarization beam combiner (PBC). The quadrature modulators are composed by two parallel double-nested Mach-Zehnder modulator (DN-MZM) [35, Ch. 7], [36] with a bandwidth greater than 30-GHz and a phase-shifter in the lower branch. In order to emulate a random data modulation, data signal was obtained using a 112-Gb/s pseudo-random bit sequence (PRBS) generator, with 12% overhead for Soft-Decision (SD) FEC.

The transmission line consists of 15 spans of 100 km of SSMF (average span loss of 20 dB) and EDFA-lumped optical amplification. The EDFAs were pumped at 980 nm to reduce the accumulated ASE noise peak occurring in the 1560–1566 nm region. The average fiber input power per channel is about +1.5 dBm/carrier. No optical fiber dispersion compensation was used in the lightpath. At the receiver side, the measured channel is selected by one tunable optical filter (TOF) with a bandwidth of 0.4 nm @1550 nm. The test channel is processed by the modified DSP showed in Fig. 6. The hardware implements polarization-and phase-diverse coherent detection with a polarization-diversity 90-degree hybrid, a tunable ECL LO (~50 kHz linewidth) and four single-ended photodetectors. The sampling and digitization was achieved by using a four ADC's with 50 GSamples/s and 20-GHz electrical bandwidth. For the DSP, we use the CMA for polarization recovery [43], [40]. In Fig. 9, we show the measured average BER of the two polarizations as a function of wavelength. One can see a comparison of BER performance with and without wavelet processing in the DSP. The 40 channels have a BER below 10^{-12}. Consequently, the wavelet processing opens the possibility
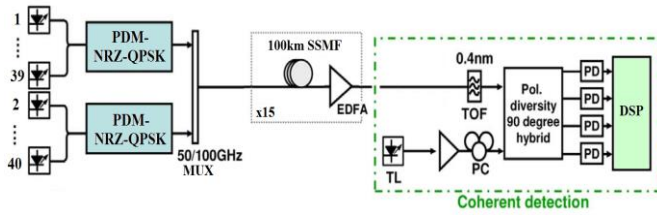
Fig. 8. Simulation scenario setup for 40 x 112-Gb/s PDM-NRZ-QPSK and coherent reception with wavelet denoising [43].
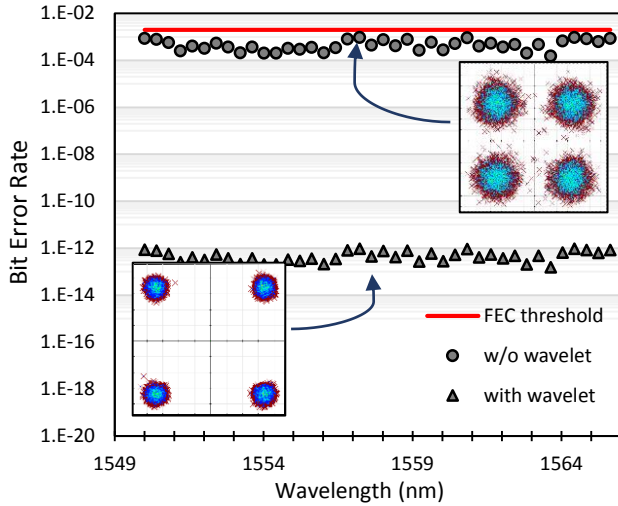

Fig. 9. BER parameter after 1500 km of transmission. Optical spectrum and the constellation diagrams of 1550 nm channel at the receiver.

of removing the FEC overhead with the additional bandwidth reduction in each WDM channel.

➤ *4.28 Bit/s/Hz, 600 km, 40x214-Gb/s PDM-CSRZ-QPSK*

In [43], the high-capacity DWDM system between Madrid and Barcelona cities of [42] was redesigned. In the first step, the work used coherent detection and optical dispersion compensation implemented by a hybrid dispersion map with double periodicity (pre-comp of -480 ps/nm, residual dispersion per span of 160 ps/nm and net residual dispersion of 0 ps/nm at 1555 nm) [42]. In the second step [43], we proposed an uncompensated transmission (UT) dispersion map and the PDM-CSRZ-DQPSK modulation format with 214-Gb/s per wavelength (14% overhead for SD-FEC) over DWDM 50-GHz grid. We demonstrated a DWDM transmission with a SE of 4 b/s/Hz without Nyquist filtering. This high-SE was achieved using commercial third-order Super-Gaussian filters and PDM-QPSK modulation format, which has a great tolerance to narrowband optical filtering.

In this subsection we maintain the design of [43] adding the wavelet denoising subsystem to the DSP located in Barcelona. Figure 10 shows the simulation scenario. At the transmitter, the architecture employed is the same as the above simulation. However, we use an additional pulse carver at the output of each conventional quadrature modulator, previous of polarization multiplexer, to convert NRZ pulses to Carrier-Suppressed Return-to-Zero (CSRZ) pulses [42]. The advantages of this PDM-QPSK version is further analyzed in [44]. On each polarization, the 110-Gb/s QPSK signals were
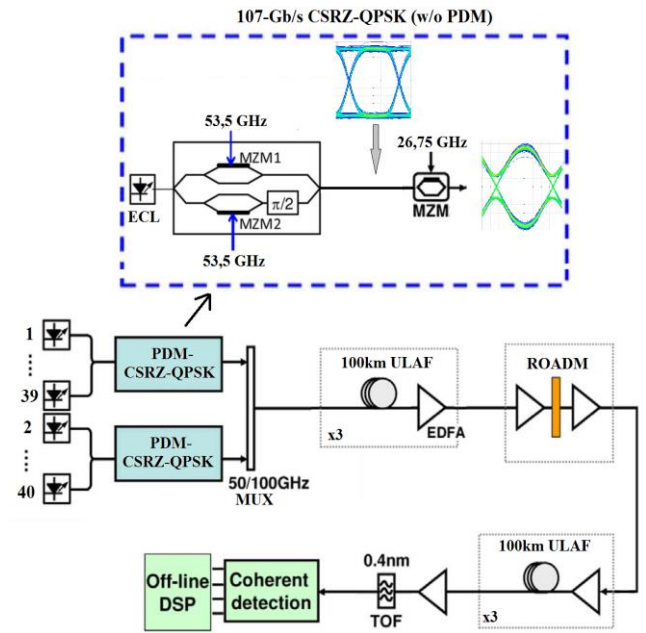

Fig. 10. DWDM optical network between Madrid and Barcelona cities. Simulation scheme proposed for 40 x 214-Gb/s PDM-CSRZ-QPSK transmission [43].
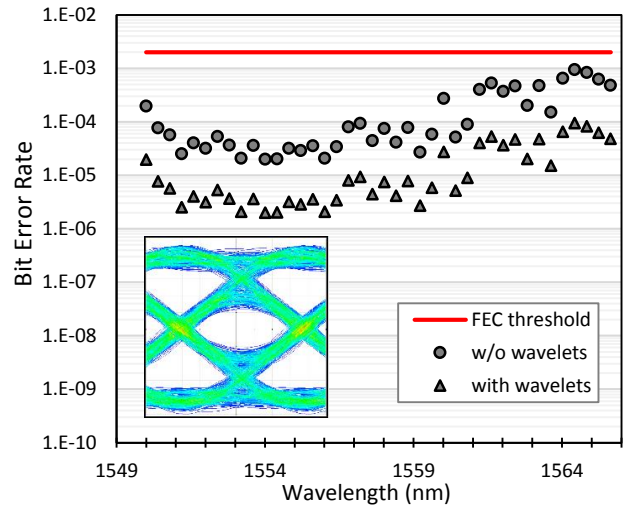

Fig. 11. Measured BER of 50-GHz spaced, 40 x 214-Gb/s PDM-CSRZ-QPSK signals after 600 km transmission with and without wavelet denoising process. The received eye diagram is inserted.

then pulse-carved with one MZM driven by 27.5-GHz clock. Additionally, a random data sequence of 65536 bits was obtained using a PRBS generator with a fixed bit rate of 214-Gb/s. The lightpath consists of 6 spans of Vascade EX2000 [13] (average span loss of 16.2 dB) with a ROADM inserted in Zaragoza. The power losses are recovered by P-EDFA amplifiers (EDFA codoped with phosphorous to increase the amplification bandwidth) pumped at 1480 nm. No optical fiber dispersion compensation was used in the network. Due to the high-effective area of Vascade EX2000 (112 μm^2) and a low Kerr nonlinear refractive index (21·10^{-21} m^2/W), we can increase the power launched to the first span from +1 to +2 dBm/wavelength. At the receiver side, the measured channel is selected by one TOF with a bandwidth of 50 GHz. The

ADC's employed have 80 GSamples/s and 40-GHz electrical bandwidth. Finally, we measured the channel performance with the DSP, which contains the wavelet denoising processing previously to the matched filter of the symbol decisor. Fig. 11 plots the BER performance comparison with and without wavelet denoising. In both cases the BER for all 40 x 214-Gb/s signals [29] were in the range from $1.9 \cdot 10^{-6}$ to $9.4 \cdot 10^{-4}$, under the enhanced FEC limitation ($\sim 2 \cdot 10^{-3}$) [15], [35, Ch. 6]. Adding the wavelet denoising operation in the DSP to increase the SNR, the BER is only slightly improved from $\sim 10^{-4}$ to $\sim 10^{-5}$. The main physical impairment is the strong ISI induce by the narrow bandpass optical filters, so the wavelet signal processing losses efficiency. The wavelet denoising technique is only effective if the ASE noise, which is AWGN, is the main limitation in the optical network.

B. Wavelets in Modal-Division Multiplexed Systems

Additionally, in collaboration with Universidad Politécnica de Valencia (UPV) and Telefónica I+D Corporation, wavelet approach has been considered for MDM researching. It is expected that some articles will be published during the next years. In this subsection, only the main reasons are mentioned for using wavelets in future MDM optical systems.

We can mention some advantages using wavelets in MDM transmissions. As we have mentioned above and according with [24], wavelet denoising process improves the SNR in optical systems where PDM-QPSK modulation format is used and ASE noise is the main optical impairment. However, in contrast with DWDM systems, in MDM transmissions the main physical impairment to obtain a high BER performance is the mode coupling between modes inducing modal crosstalk at the receiver. MIMO processing is required in the DSP to eliminate this perturbation in data transmitted. Additionally to MIMO processing, wavelets have been proposed to minimize the mode coupling in few-mode and multimode fibers. In some works ([33], [39], [27], [48]) wavelets have been studied using them as a new scheme of encoding data bits. The approach is to use specific wavelet functions instead of NRZ, RZ or CSRZ pulses in combination with advanced modulation formats to reduce the mode coupling and the modal crosstalk.

In [25], the wavelets based on Shifted Prolate Wave Spheroidal functions (SPWS) have been analyzed. Now, in this work these functions are proposed to reduce the modal interference based on their electromagnetic properties [38]. The SPWS functions have the property of being four-dimensional orthogonally, i.e. four different SPWS functions which are modulated by four independent wavelengths or modes are orthogonal to each other. Consequently, it can be expected that the use of these functions will reduce the phase perturbations induced by mode coupling in the transmitted signals. The SPWS functions have a finite spectrum in the band $[\omega_0 - \Omega/2, \omega_0 + \Omega/2]$ and the minimal effective temporal duration T. The dual-orthogonality condition is satisfied:

$$\int_{-\infty}^{+\infty} \psi_i(t)\psi_j(t)dt = \begin{cases} 0, & i \neq j \\ 1, & i = j \end{cases} \tag{22}$$
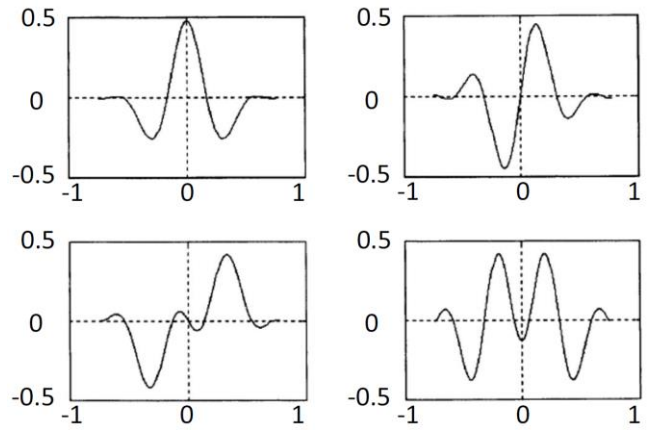

Fig. 12. The Shifted Prolate Wave Spheroidal (SPWS) basic functions (or mother wavelets) proposed to reduce the modal crosstalk in MDM transmissions.

$$\int_{-T/2}^{+T/2} \psi_i(t)\psi_j(t)dt = \begin{cases} 0, & i \neq j \\ \lambda_i, & i = j \end{cases} \tag{23}$$

Three basic functions reach the 99% of the energy in $\Omega T/2=7$, and four basic functions in $\Omega T/2=9$. The four basic functions (also known as mother wavelets) of four-dimensional vector sub-space are plotted in Fig. 12. The use of these functions in each optical carrier or mode reduces the modal crosstalk and the mode coupling, allowing us to reduce the spectral separation among the above optical carriers. As a result, the SE is maximized.

IV. WAVELET-BASED FILTERING FOR FIBER BACKWARD-PROPAGATION IN DWDM SYSTEMS

One of the benefits associated with coherent optical transmission systems is the possibility to obtain higher SE compared to classical direct-detection optical systems. The increase in SE for long-haul transmissions is usually accompanied by higher power launched to the fiber, which degrades the BER performance due to fiber Kerr nonlinearities [4], [5]. Mitigation of nonlinear effects can be achieved by using dispersion-managed systems [55], but this solution introduces added noise and is quite rigid. Alternatively, digital signal processing (DSP) may be used to achieve backward-propagation, as explained in the following.

The concept of backward-propagating an optical signal to mitigate transmission effect stems from Yariv et al. which in 1979 suggested the use of phase-conjugation for dispersion compensation [3]. Fisher et al. extended this notion in 1983 to compensate for both dispersion and Kerr nonlinearity [45]. The use of a medium with negative nonlinear index (e.g., semiconductors) to reverse the effects of transmission without phase conjugation was suggested in [10]. An examination of the nonlinear Schrödinger equation (NLSE), which governs the evolution of optical signal propagation in fiber with Kerr nonlinearity, reveals that all these techniques amount to reversing the fiber parameters (either dispersion, nonlinear index, or both). This is mathematically equivalent to reversing the spatial variable sign in the NLSE and hence the technique

is referred to as backward-propagation. Comparing post-compensation versus pre-compensation techniques via backward-propagation, the former takes into account all deterministic effects in fiber, allowing the use of conventional transmitter architecture and offering flexibility through adaptive processing.

On the other hand, an efficient real-time implementation of any DSP algorithm in a communication system context is crucial in order to reduce transmission latency and power consumption. Finite impulse response (FIR) filtering is highly compatible with real-time DSP implementation, as compared to infinite impulse response (IIR) filtering. It does, however, suffer from limited efficiency [35, Ch.5]. In [20] and [21], the authors suggest a wavelet-based FIR filter design used for backward-propagation, which is shown to achieve higher efficiency compared to alternative filter design procedures. In this section, the main ideas of that work are revised.

A. The split-step method for backward-propagation

Backward propagation is achieved using DSP after coherent detection the received signal is backward-propagated by solving the NLSE with the spatial variable negated:

$$\frac{\partial A}{\partial(-z)} = (\hat{D} + \hat{N})A \tag{24}$$

where A is the complex electric field, $\hat{D}$ is the linear operator accounting for dispersion as well as fiber loss and $\hat{N}$ is the nonlinear operator, which takes Kerr nonlinearity into account. These operators are given by:

$$\hat{D} = -j\frac{\beta_2}{2}\frac{\partial^2}{\partial t^2} + \frac{\beta_3}{6}\frac{\partial^3}{\partial t^3} - \frac{\alpha}{2} \tag{25}$$

$$\hat{N} = j\gamma|A|^2 \tag{26}$$

where α, β_2, β_3 and γ are the attenuation factor, first- and second-order group-velocity dispersion and the nonlinearity parameter, respectively. To solve (20), each fiber span is divided into N_{step} steps, each of z_{step} length. The ligthpath length for N_{spans} is $L = N_{spans}z_{span} = N_{spans}N_{step}z_{step}$. At each step the corresponding (25) and (26) equations are solved. Fiber loss is accounted for at each step, while amplification is reversed before each span. Backward-propagation for a single span using this approach is illustrated in Fig. 13. As we have mentioned above FIR filtering is practical in comparison with IIR filtering due to FIR approach does not require buffering [35, Ch.5]. The FIR filter coefficients may be obtained by an inverse-Fourier transform (IFT) of the dispersion frequency response of each step. This makes the filter length identical to the IFT length, which should be made long enough to achieve high accuracy in the linear and nonlinear compensation. To reduce the computational load in the DSP time-domain windowing of the dispersion compensating FIR filter may be considered; e.g., using Tukey windowing [58]. There is however, a fundamental issue associated with windowing of the FIR filter: the loss of the all-pass property of the dispersion operator. As multiple steps of dispersion compensation are
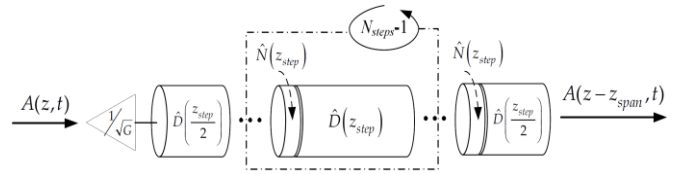

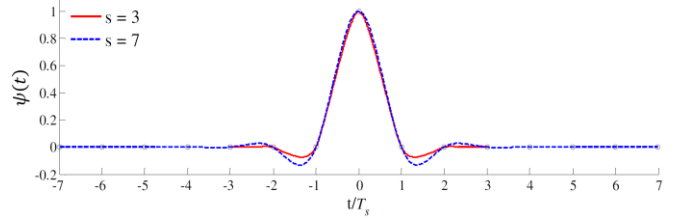Fig. 13. Single span backward-propagation. This figure is inserted from [20].

Fig. 14. Mother wavelet with $s = 3, 7$. This figure is inserted from [20].

required, the accumulated error from the windowing of the FIR filter becomes significant and the ultimate quality of the backward-propagated signal is deteriorated. IFT-based design of the FIR dispersion compensation filter is suboptimal since the Fourier transform relies on a harmonic decomposition basis which is not time-limited and windowing is hence required. Wavelet-based filter design of the dispersion operator is based on time-limited decomposition. This approach is shown to achieve accurate back-propagation while reducing the number of operations required for the linear operator.

B. Wavelet filtering

In wavelet decomposition temporal limited basic functions are employed. As suggested in [51], a possible choice for the decomposition basis is the Deslaurier-Duruc interpolating scaling function $\psi(t)$. The function's support is determined by a single parameter s. The compact-support property is stated as $\psi(t) \equiv 0, \forall|t| > sT_s$, where T_s is the sample period. The interpolating scaling function is defined by a filter whose coefficients are given by [20], [21], [51]:

$$h_{2k} = \delta_k \tag{27}$$

$$h_{2k+1} = \frac{(-1)^{\frac{s+1}{2}-k}\prod_{q=0}^{s}\left(q - \frac{s}{2}\right)}{\left(\frac{s-1}{2}-k\right)!\left(\frac{s+1}{2}+k\right)!\left(k+\frac{1}{2}\right)} \tag{28}$$

where δ_k is the delta function and $h_{2k+1} = h_{-(2k+1)}$. The compact support of the mother wavelet $\psi(t)$ determinates that $h_k \equiv 0, \forall|k| > s$. The parameter s is used to match the dispersion compensating filter length to the required dispersion-induced pulse spreading time-frame. An example is illustrated in Fig. 14 to $s = 3, 7$.

To compensate the second and third order chromatic dispersion degradation in the optical pulses, it is necessary to calculate the second and third order derivatives of the time-shifted wavelet function $\psi_m(t) = \psi(t - mT_s)$. To achieve this, the following set of equations is to be solved:

$$\sum_{k=-(s+1)/2}^{(s-1)/2} h_{2k+1} D_{2(k+n)+1}^{(\mu)} - 2^{-\mu} D_n^{(\mu)} + D_{2n}^{(\mu)} = 0 \quad (29)$$

$$\sum_{n=1-s}^{s-1} n^{\mu} D_n^{(\mu)} = \mu! \quad (30)$$

where n is an integer and Eq. (5b) is used for normalization. There are s equations required to obtain $\overrightarrow{D^{(\mu)}}$. The Wavelet-based FIR filter used for dispersion compensation is given by the following equation, where an extension from [51] to introduce second-order group-velocity dispersion is included:

$$\overrightarrow{h_f} = IFFT\left\{ exp\left\{ \left\{ FFT\left[\frac{1}{2T_s^2}\left(-j\beta_2 \overrightarrow{D^{(2)}} + \frac{\beta_3 \overrightarrow{D^{(3)}}}{3T_s} \right) \right] + \frac{\alpha}{2} \right\} z_{step} \right\} \right\}$$

(31)

In order for $\overrightarrow{h_f}$ to obtain high accuracy, $\overrightarrow{D^{(2,3)}}$ are zero-padded (before the FFT) so that the impulse response is longer than IFT/Tukey windowing approach. For this reason, $\overrightarrow{h_f}$ is truncated to allow savings in number of operations by setting all the coefficients that result in $log\{|\overrightarrow{h_f}|\} < \varepsilon$ to zero. ε parameter may be scanned to obtain a value which allows good performance while minimizing the number of non-zero $\overrightarrow{h_f}$ coefficients.

C. Simulation, results and discussion

In [20], Goldfarb *et al.*, performed a DWDM simulation of 9 QPSK channels at 10 Gbaud (20-Gb/s) with 20 GHz channel spacing. At the transmitter a pseudo-random bit sequence of order 23 was employed. The lightpath consists in 48 x 100 km spans with non-zero dispersion shifted fiber (NZDSF+). The main fiber parameters are: α = 0.2 dB/km, D = 4 ps/nm·km, S = 0.045 ps/nm²·km and γ = 1.46 (W·km)⁻¹. EDFA-lumped amplification was used to compensate the fiber losses with a noise figure of 5 dB. At the receiver, optical coherent detection was employed with a sampling rate in the ADC's of 320 GHz (T_s = 3.125 ps). The sampling rate is selected with a disproportional value in comparison with commercial analog-to-digital converters [54] due to simulation reasons. The optimum total launching power is found to be 5 dBm and a step size of 2 km was determined to achieve close to zero penalty performance.

A comparison of three FIR filters using IFT, IFT with Tukey windowing (both in frequency and time, as in [51]) and wavelet-based design is seen in Fig. 15. The impulse response is plotted on a logarithmic scale for clarity. The plot reveals the slow decay of the IFT filter; Tukey windowing limits the extent (and hence the number of operations required for filtering) of the IFT-based filter. Wavelets-based design achieves tighter windowing limits due to the compact-support of the decomposition function it is based upon. Moreover, observing the transfer function comparison between IFT/Tukey and wavelets-based designs (Fig. 15, lower graph)
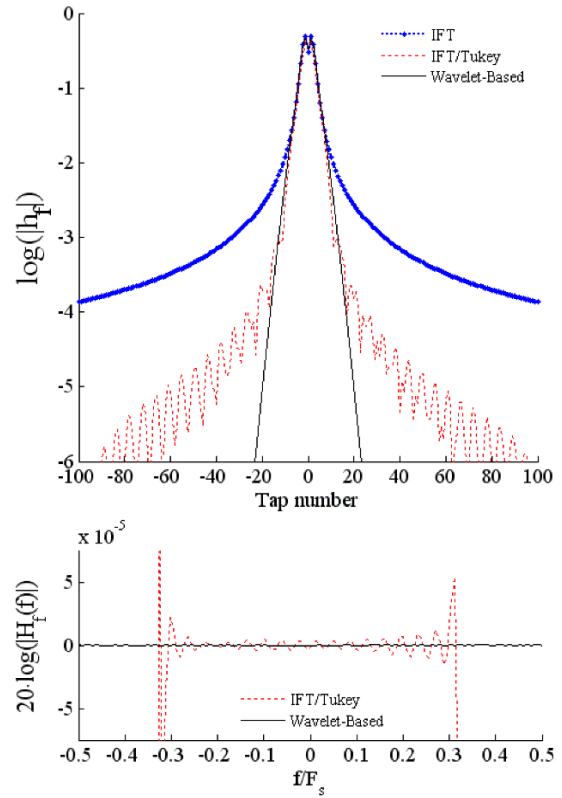

Fig. 15. Impulse response of dispersion compensation FIR filter with IFT, IFT/Tukey and wavelets-based designs (upper graph), transfer function in logarithmic scale (lower graph). This figure is inserted from [20].
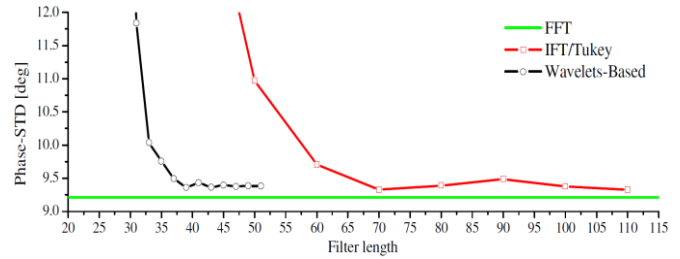

Fig. 16. Performance comparison of IFT/Tukey and wavelets-based FIR filter design as a function of filter length. This figure is inserted from [21].

shows that the all-pass characteristic of the wavelet-based filter is preserved much better than with the IFT/Tukey design. Loss of the all-pass feature combined with multiple linear compensation operations required when employing the SSM is a significantly severe issue.

A performance comparison of the two filter designs is shown in Fig. 16. It is observed that the wavelets-based FIR filtering approach achieves equivalent performance as the IFT/Tukey design (both being close to the frequency-domain linear compensation implementation). The wavelet-based filter achieves this performance using 39 taps, as opposed to 70 taps for the IFT/Tukey design. The number of filter taps required for the linear operator is hence reduced by a factor of approximately 1.8, validating the wavelet-based approach to dispersion-compensation FIR filter design. Although the wavelets-based is more efficient than IFT-based ones, the

implementation of backward-propagation leads to a larger computational load and latency, compared to lumped linear compensation only. The backward-propagation scheme's additional computational load and latency should be taken into account as an engineering trade-off with its superior performance, compared to linear compensation only.

V. FUTURE PERSPECTIVES: ALL-OPTICAL WT

In classical digital and optical communication, Fourier signal processing based in temporal non-limited harmonic functions has predominated [4], [30]. However, wavelet signal decomposition has been recently proposed with the two approaches mentioned in Section III. The first approach, related to wavelet signal denoising process, is the most relevant for future researches and commercialization of new products and services. Its advantages in terms of SNR improvement in DWDM transmissions make it an attractive candidate for the scientific community.

The wavelet denoising process described in [24] involves a linear discrete wavelet transform, a nonlinear thresholding step and a linear inverse discrete wavelet transform. These operations are inserted previously to the matched filter inside of the coherent optical receiver (Figures 6 and 17). However, the electrical circuits are currently reaching their bandwidth limits due to the continuous increase of data traffic. Therefore, the implementation of all-optical circuits for time domain signal processing could help overcome the severe speed limitations that are currently imposed by electronics solutions in networking systems. All-optical systems offer the potential for larger bandwidth: the available bandwidth in an optical fiber in the low-loss telecommunication spectral range from 1300 nm to 1600 nm is ≈ 40 THz, compared to a few gigahertz for electronic systems. Here, we propose to move the electrical DWT to all-optical wavelet transform design in a first step due to the complexity of the complete migration. The implementation of all-optical wavelet denoising process is relegated to future works.

The wavelet transform in the optical domain is referred as *"all-optical WT"*. Its implementation requires to consider the continuous wavelet transform (CWT) in contrast with the discrete nature of this transform in the electrical domain due to the sampling of the received signal in the previous ADCs. Consequently, the WT is moved from the DSP to precede the coherent detection, between the optical band pass filter and the photodiodes as we have illustrated in Fig. 18. This optical operation is performed with a signal wavelet generator [61], an optical mixer [49] [50] and an optical integrator [8]. The basic structure is plotted in Fig. 19. The first subsystem generates the mother wavelet with the corresponding *delay&scale* (n,m). The wavelet temporal profile is obtained based on PM–IM conversion in an optical frequency discriminator [28]. The lightwave from an LD is fed to an optical phase modulator that is driven by an electrical Gaussian pulse. The phase-modulated optical signal is then applied to an FBG via an optical circulator. The PM–IM conversion is achieved by using the FBG serving as a frequency discriminator [61], [8]. The optical mixer is implemented via an optical coupler and a Proustite crystal, where is induced the three-wave mixing [49]. The output is
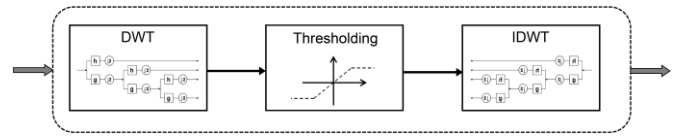

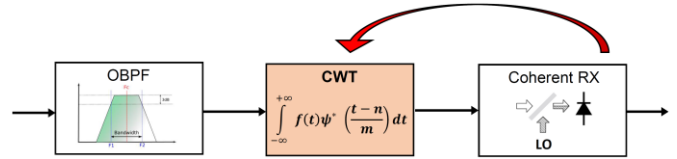Fig. 17. Wavelet denoising subsystems.

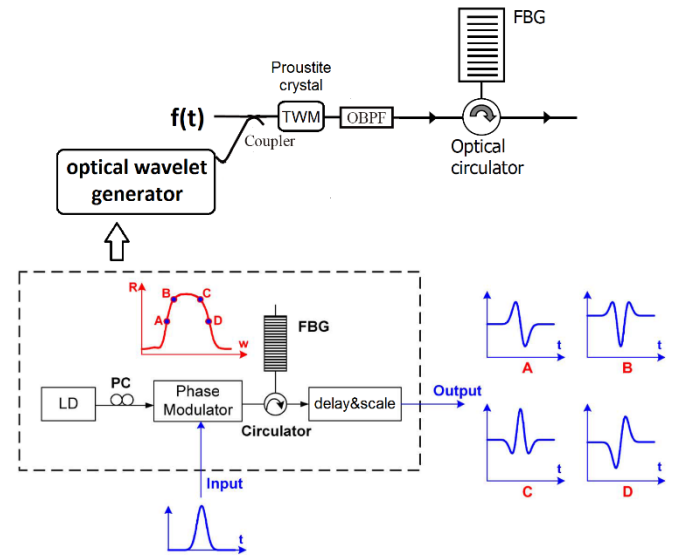Fig. 18. First subsystem of wavelet denoising process moved to optical domain.

Fig. 19. All-optical continuous wavelet transform design.

filtered by an optical bandpass filter (OBPF) to avoid the undesirable frequencies generated by this nonlinearity. The implementation of the optical mixer involving nonlinearities makes this design energy inefficient. Therefore, the main open issue is to redesign the optical mixing with a passive device to do this subsystem energy efficient. Finally, the integral operation is achieved by a fiber Bragg grating (FBG) and an optical circulator according to Azaña's studies in [8].

Returning to the use of wavelets with the proposal explained in Section IV (second approach), the main challenges to the future are the migration to superchannels transmissions [9] and SDM technologies [35]. The wavelet-based filtering for fiber backward-propagation should be compatible with multicore and multimode transmissions.

VI. CONCLUSIONS

In this paper, we have attempted to outline the main applications of wavelet signal processing in currently DWDM and future MDM optical systems. In contrast with Fourier signal decomposition, wavelet transform is based in temporal and spectral limited non-harmonic functions. The mathematic fundamentals have been reviewed in Section II.

According to several authors, wavelets in DWDM systems have been proposed with two different proposals. The first is the wavelet signal denoising procedure (DWT + threshold + IDWT), which is inserted previously to the matched filter inside of the coherent optical receiver. Using the Daubechies5 and Haar wavelets improvements in BER of over three orders of magnitude are achievable within the range of E_b/N_0 from -5 dB to 8 dB for QPSK modulation. The second proposal is the wavelet-filtering used for linear and nonlinear compensation in the backward-propagation scheme, which is shown to achieve a higher computational efficiency compared to classical filter design procedures.

In MDM transmissions SPWS wavelets have been proposed to minimize the mode coupling in FMF and MMF. The Shifted Prolate Wave Spheroidal functions have the property of being four-dimensional orthogonally. If independent optical carriers or modes are modulated by different SPWS functions they will be orthogonal to each other and the mode coupling will be reduced maximizing the SE.

In the last part of this work the wavelet denoising design is reviewed. The electrical domain is limited in bandwidth to a few gigahertz. For this reason the migration to the optical domain is proposed redesigning the WT with optical devices, which is known as *"all-optical WT"*. An optical mixer and an optical integrator based on FBG are employed to implement this signal transform.

REFERENCES

[1] A. N. Akansu and R. A. Haddad, "Multiresolution Signal Decomposition: Transforms, Subbands, and Wavelets", 2nd ed. Newark, NJ: New Jersey Institute of Technology, 2001

[2] A. Vgenis, C. Petrou, C. Papadias, I. Roudas, and L. Raptis, "Nonsingular constant modulus equalizer for PDM-QPSK coherent optical receivers," in IEEE Photon. Technol. Lett., vol. 22, no. 1, pp. 45–47, Jan. 1, 2010.

[3] A. Yariv, D. Fekete, and D. M. Pepper, "Compensation for channel dispersion by nonlinear optical phase conjugation," Opt. Lett. 4, 52–54 (1979).

[4] Agrawal, G.P., "Fiber-Optic Communication Systems", Wiley Interscience, Four Edition, 2010.

[5] Agrawal, P.G., "Nonlinear Fiber Optics", San Diego: Elsevier Science & Technology, 5th edition, 2013.

[6] Akhil R. Shah, Rick C. J. Hsu, Alireza Tarighat, Ali H. Sayed and Bahram Jalali, "Coherent Optical MIMO (CO-MIMO)", in J. Lightw. Technol., vol. 23, no. 8, Aug., 2005.

[7] Ayhan, Y. and Cavdar, I.H., "Optimum link distance determination for a constant signal to noise ratio in M-ary PSK modulated coherent optical OFDM systems", in Telecommunication Systems, August, 2013.

[8] Azaña, J., "Waveguide (Fiber) - Based Ultrafast All-Optical Signal Processors", conference in CSIC (Madrid), January 2014.

[9] Bennett, G., "Superchannels to the rescue", in J. Lightw. Technol., from March/April 2012.

[10] C. Pare, A. Villeneuve, P. A. Belanger, and N. J. Doran, "Compensating for dispersion and the nonlinear Kerr effect without phase conjugation," Opt. Lett. 21, 459-461 (1996).

[11] C. S. Burrus, R. A. Gopinath, and H. Guo, "Introduction to Wavelets and Wavelet Transforms". Englewood Cliffs, NJ: Prentice Hall, 1998.

[12] Corning Incorporated, "Datasheet Corning® SMF-28e+® Optical Fiber", 2011.

[13] Corning Incorporated, "Datasheet Corning® Vascade® Optical Fibers", 2010.

[14] D. Godard, "Self-recovering equalization and carrier tracking in twodimensional data communication systems," IEEE Trans. Commun., vol. 28, no. 11, pp. 1867–1875, Nov. 1980.

[15] Djordjevic, I.B., Arabaci, M. and Minkov, L.L., "Next Generation FEC for High-Capacity Communication in Optical Transport Networks", in J. Lightw. Technol., vol. 27, no. 16, Aug. 15, 2009.

[16] E. Ip and J. Kahn, "Feedforward carrier recovery for coherent optical communications," J. Lightw. Technol., vol. 25, no. 9, pp. 2675–2692, Sep. 2007.

[17] Essiambre, R.J., Kramer, G., Winzer, P.J., Foschini, G.J. and Goebel, B., "Capacity Limits of Optical Fiber Networks", in J. Lightw. Technol., vol. 28, nº 4, February 15, 2010.

[18] F. Yaman and G. Li, "Nonlinear impairment compensation for polarization-division multiplexed WDM transmission using digital backward propagation," in IEEE Photon. J., vol. 1, no. 2, pp. 144–152, Aug. 2009.

[19] G. Beylkin, "On the Representation of Operators in Bases of Compactly Supported Wavelets", in SIAM J. on Numerical Analysis 29, 1716-1740 (1992).

[20] G. Goldfarb and G. Li, "Efficient backward-propagation using wavelet based filtering for fiber backward-propagation," in Opt. Exp., vol. 17, no. 11, pp. 8815–8821, 2009.

[21] G. Goldfarb and G. Li, "Wavelet Split-Step Backward-Propagation for Efficient Post-Compensation of WDM Transmission Impairments", in Optical Fiber Communications Conference (OFC), March 2009.

[22] G. Goldfarb, M. G. Taylor, and G. Li, "Experimental Demonstration of Fiber Impairment Compensation Using the Split-Step Finite-Impulse-Response Filtering Method", in IEEE Photon. Technol. Lett. 20, 1887-1889 (2008).

[23] G. Strang and T. Nguyen, "Wavelets and Filter Banks". Wellesley, MA: Wellesley-Cambridge Press, 1996

[24] Ge, Y. and Daut, D.G., "Bit Error Rate Analysis of Digital Communications Signal Demodulation Using Wavelet Denoising", in Sarnoff Symposium, 34th IEEE, 2011.

[25] Gilbert, G.W. and Xiaoping, S., "Wavelets Based on Prolate Spheroidal Wave Functions", in Fourier Analysis and Applications Journal, vol. 10, issue 1, 2004.

[26] Guifang Li, "Recent Advances in Coherent Optical Communications", in Advances in Optics and Photonics 1, pp.279-307, OSA (Optical Society of America), 2009.

[27] Gupta, D., Vats, V.B. and Garg, K.K., "Performance Analysis of DFT-OFDM, DCT-OFDM, and DWT-OFDM Systems in AWGN Channel", in the Fourth International Conference on Wireless and Mobile Communications, 2008.

[28] H. Asghari, M.H., Park, Y., Dai, Y., Yao, J. and Azaña, J., "New Concept for Ultra-broadband Photonic Integrator with Fundamentally Unlimited Operation Time Window", in the Conference on Lasers and Electro-Optics (CLEO), 2009.

[29] ITU-T G.694.1 Recommendation (2012), "Spectral grids for WDM applications: DWDM frequency grid".

[30] J. G. Proakis, Digital Communications, 4th ed. New York: McGraw-Hill, 2001.

[31] J. Navarro and D. Elizarraraz, "Introducción a la Transformada Wavelet Continua". Reverté-UAM, 2010

[32] J. Walker, "A primer on wavelets and their scientific applications", 2nd edition, chapman Hall/CRC, 2008

[33] Jones, W.W., "Multi-scale wavelet modulation", in Proceedings of the 26th Southeastern Symposium on System Theory, 1994.

[34] K. M. Ho, C. Vaz and D. G. Daut, "Improved Demodulation of Phase Shift Keyed Signals Using Wavelet Thresholding", in Proc. 2008 Sarnoff Symp., Princeton, NJ, April 28-30, 2008.

[35] Kaminow, I.P., Li, T. and Willner, A.E., "Optical Fiber Telecommunications VIB", Elsevier, Six Edition, 2013.

[36] Keang-Po Ho, "Phase-Modulated Optical Communications Systems", Springer, 2005.

[37] Li, L., Jijun, Z., Degong, D. and Aihan, Y., "Analysis modulation formats of DQPSK in WDM-PON system", in Optik, vol. 123, pp. 2050-2055, 2012.

[38] Li, L.-W., Kang, X.-K. and Leong, M.-S., "Spheroidal Wave Functions in Electromagnetic Theory", John Wiley & Sons, First Edition, 2002.

[39] Lindsey, A.R. and Dill, J.C., "Wavelet packet modulation: a generalized method for orthogonally multiplexed communications", in Proceedings

of the Twenty-Seventh Southeastern Symposium on System Theory, 1995.

[40] M. Kuschnerov, F. Hauske, K. Piyawanno, B. Spinnler, M. Alfiad, A. Napoli, and B. Lankl, "DSP for coherent single-carrier receivers", in J. Lightw. Technol., vol. 27, no. 16, pp. 3614–3622, Aug. 15, 2009.

[41] M. V. Wickerhauser, "Adapted Wavelet Analysis from Theory to Software", A. K. Peters, Ltd., Wellesley, MA, 1994.

[42] Macho, A., "Comunicaciones Ópticas de Banda Ancha con Fase Modulada: Estudio de la Degradación de la Señal Óptica", Final Project Degree, Professor: Paloma Rodríguez Horche, Universidad Politécnica de Madrid, Photonic Technology Department, 2013. Available in Archivo Digital UPM (http://oa.upm.es/).

[43] Macho, A., "Digital Coherent Receivers and Advanced Optical Modulation Formats in 100 and 200 Gb/s DWDM Systems", final work for the course Sistemas Avanzados de Comunicaciones, ETSIT-UPM, Madrid (Spain), 2014. Available in Archivo Digital UPM (http://oa.upm.es/).

[44] Macho, A., Horche, P., "Pulse-Shape Analysis in 100 and 200 Gb/s PDM-(D)QPSK DWDM Systems", in Optik Journal (expected to be published in 2015).

[45] R.A. Fisher, B. R. Suydam, and D. Yevick, "Optical phase conjugation for time-domain undoing of dispersive self-phase-modulation effects," Opt. Lett. 12, 611-613 (1983).

[46] S. G. Mallat, A "Wavelet Tour of Signal Processing", Third Edition: The Sparse Way, 1999

[47] S. J. Savory, "Digital filters for coherent optical receivers," Opt. Exp., vol. 16, no. 2, pp. 804–817, 2008.

[48] S.Ananthi, K.Padmanabhan and K.R.Balaje, "A different scheme of encoding data bits in Digital Communication using Wavelets", 978-1-4673-5301-4/13/$31.00 ©2013 IEEE.

[49] Saleh, B.A.E. and Teich, M.C., "Fundamentals of Photonics" John Wiley & Sons, Second Edition, 2007.

[50] T. Fujita, Y. Toba, Y. Miyoshi and M. Ohashi, "Optical Analog Multiplier based on Phase Sensitive Amplification", in OptoElectronics and Communications Conference held jointly with International Conference on Photonics in Switching (OECC/PS), 2013.

[51] T. Kremp and W. Freude, "Fast split-step wavelet collocation method for WDM system parameter optimization", in J. Lightwave Technol. 23, 1491-1502 (2005).

[52] Vizcaíno, J.L., Ye, Y., Jiménez. F., Macho. A. and Krummrich, P.M., "Optimized Amplifier Placements for Improved Energy and Spectral Efficiency in Protected Mixed-Line-Rate Networks", in Optical Fiber Communications Conference (OFC), March 2014.

[53] Vizcaíno, J.L., Ye, Y., Macho. A., Jiménez. F. and Krummrich, P.M., "Increased Energy-efficiency and Capacity for Mixed-Line-Rate WDM Networks with Additional Hybrid EDFA-Raman", in European Conference Optical Communications (ECOC), excepted to be published in Nov. 2014.

[54] Walden, R.H., "Analog-to-digital converters and associated IC technologies" in Proc. Compound Semicond. Integr. Circuits. Symp., pp.1-2, 2008.

[55] Winzer, P.J. and Essiambre, R.J., "Advanced optical modulation formats", Proc. IEEE, vol.94, nº 5, pp.952-985, May 2006.

[56] Winzer, P.J. and Essiambre, R.J., "Advanced optical modulation formats", in Optical Fiber Telecommunications, 2008.

[57] Winzer, P.J., "High-Spectral-Efficiency Optical Modulation Formats", in J. Lightw. Technol., vol. 30, nº 24, December 15, 2012.

[58] X. Li, C. Xingzhong, and M. Qasmi, "A broad-band digital filtering approach for time-domain Simulation of pulse propagation in optical fiber", in J. Lightwave Technol. 23, 864-875 (2005).

[59] X. Wu, J. Jargon, Willner, A.E. "Off-Line Monitoring of OSNR/CD/PMD Degradation Effects Using Neural-Network-Based Training Sequences", in European Conference Optical Communications (ECOC), 2008.

[60] Y. Miyamoto, "High-Capacity Scalable Optical Communication for Future Optical Transport Network", ISSCC 2014

[61] Yao, J., Zeng, F. and Wang, Q., "Photonic Generation of Ultrawideband Signals", in J. Lightw. Technol., vol. 25, no. 11, 2007.

[62] Yu, J., Dong, Z., Chien, H.-C., Jia, Z., Li, X., Huo, D., Gunkel, M., Wagner, P., Mayer, H. and Schippel, A., "Transmission of 200 G PDM-CSRZ-QPSK and PDM-16QAM with a SE of 4 b/s/Hz", in J. Lightw. Technol., vol. 31, nº 4, February 15, 2013.

[63] Zhou, X. and Yu, J., "Multi-Level, Multi-Dimensional Coding for High-Speed and High-Spectral-Efficiency Optical Transmission", in J. Lightw. Technol., vol. 27, nº 16, August 15, 2009.

Andrés Macho received the Telecommunication Engineering degree (M.S.) from the ETSIT-Universidad Politécnica de Madrid in 2013. Currently, he is working towards his Ph.D. degree at Nanophotonics Technology Center Universidad Politécnica de Valencia (Spain). His professional interest includes high-capacity wavelength-division multiplexed systems (WDM), advanced optical modulation formats and space-division multiplexing for optical networks. He worked in 2013 at Telefonica R&D Corporation in the Core Network Evolution group involved in some R&D European projects (INSPACE, STRAUSS and DISCUS).